Determination of III-V/Si absolute interface energies: Impact on wetting properties

S Pallikkara Chandrasekharan, I Lucci, D Gupta, C Cornet, L Pedesseau

Determination of III-V/Si absolute interface energies: Impact on wetting properties

S. Pallikkara Chandrasekharan, I. Lucci, D. Gupta, C. Cornet, and L. Pedesseau*
Université de Rennes, Institut National des Science Appliquées (INSA) Rennes, Centre National de la Recherche Scientifique (CNRS), Institut FOTON, UMR 6082, F-35000 Rennes, France

(Received 29 March 2023; revised 25 July 2023; accepted 28 July 2023; published 21 August 2023)

Here, we quantitatively determine the impact of III-V/Si interface atomic configuration on the wetting properties of the system. Based on a description at the atomic scale using density functional theory, we first show that it is possible to determine the absolute interface energies in heterogeneous materials systems. A large variety of absolute GaP surface energies and GaP/Si interface energies are then computed, confirming the large stability of charge-compensated III-V/Si interfaces with an energy as low as 23 meV/Å^2. While stable compensated III-V/Si interfaces are expected to promote complete wetting conditions, it is found that this can be easily counterbalanced by the substrate initial passivation, which favors partial wetting conditions.

DOI: 10.1103/PhysRevB.108.075305

I. INTRODUCTION

The epitaxial integration of dissimilar materials with different physical properties is one of the greatest challenges in materials science, as it enables the development of multifunctional devices. A large variety of materials associations has been attempted by several groups, e.g., oxides/III-V [1], oxides/Si [2], III−V/Si [3], III−V/Ge [4], and hybrid perovskites/PbS [5]. However, it is also well known that the performances of photonic or energy harvesting devices developed with such heterogeneous material associations strongly depend on materials defects that are generated at the hybrid interface [3,6–9]. Fundamentally, at hybrid interfaces, the mechanical stacking of atoms is constrained by the chemical mismatch between the atoms of the substrate and those of the deposited layer. The real atomic arrangement at hybrid interfaces is very hard to determine experimentally, although it has drastic consequences on their physical properties, such as electronic wave functions; spatial extents; dielectric, vibrational, or transport properties; and band bendings near the interface (see, e.g., [10]). Nevertheless, *ab initio* atomistic calculations have previously been used to assess the relative stability of several comparable heterogeneous interfaces in the III-V/Si model case: GaP/Si [11–13]. Especially the relative stability of abrupt III-Si or V-Si interfaces and charge-compensated interdiffused interfaces (where group III or V atoms are mixed with Si ones within one or a few monolayers) has been discussed in detail [10–12,14]. In those previous works, the authors explained the good stability of charge-compensated interfaces by using the electron counting model (ECM) criteria [15]. A very recent analysis of the high-resolution transmission electron microscopy of the GaP/Si interface confirmed the probable formation of Ga-compensated interfaces [16].

This approach is particularly interesting, as it challenges the conventional description of III-V/Si epitaxial integration which usually considers that, once a monoatomic layer is sent to the substrate surface, it remains stuck without any evolution or change during subsequent layer growth. However, at typical epitaxial temperatures (> 400 °C), the reorganization of the interface atomic arrangement is indeed very probable.

While the authors previously pointed out a very important criterion for interface stability [7–9,11], the lack of any absolute quantitative estimation of the interface energy hampers the clarification of partial/total wetting conditions, which strongly impact the defects generation [3]. Indeed, the determination of the Young-Dupré spreading parameter Ω [17] requires the quantitative knowledge of both surface and interface energies, which was preliminarily done for abrupt interfaces only [3]. In the case of III-V/Si, this parameter is given by [3]

$$\Omega = \gamma^S_{(\mathrm{Si})} - \gamma^S_{(\mathrm{III-V})} - \gamma^i_{(\mathrm{III-V/Si})}, \tag{1}$$

where $\gamma^S_{(\mathrm{III-V})}$ and $\gamma^S_{(\mathrm{Si})}$ are the surface energies of the most stable III-V facet that would be involved in the two-dimensional (2D) growth on the substrate and of the silicon surface, respectively, and $\gamma^i_{(\mathrm{III-V/Si})}$ is the interface energy between the III-V semiconductor and Si. A positive value of Ω corresponds to perfect wetting conditions, while a negative value corresponds to partial wetting, i.e., a Volmer-Weber growth, or perfect nonwetting conditions.

In this paper, we first show how absolute interface energies can be computed for heterogeneous material associations by using density functional theory (DFT). We then determine the absolute interface energies for different abrupt and compensated GaP-Si interfaces. We finally discuss the impact of the interface atomic structure on the wetting properties of III-V semiconductors on Si.

*Corresponding author: laurent.pedesseau@insa-rennes.fr

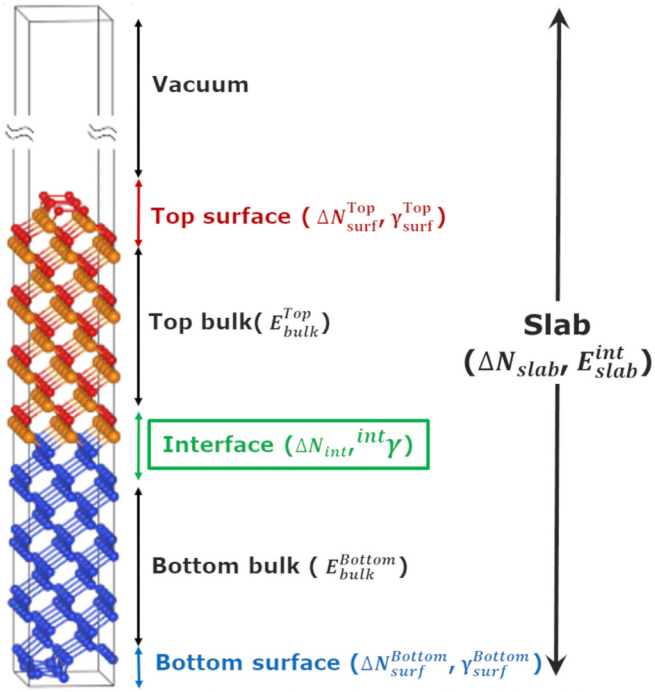

FIG. 1. Schematic of a supercell used for absolute interface energy determination, where the most important energy contributions E and γ are identified. Excess or lack of atoms induced by the surfaces and the interface as compared with the bulk is given by the deviation to the bulk stoichiometry ΔN.

II. GENERAL STRATEGY

Here, we propose using DFT to numerically evaluate the absolute interface energy. To this aim, two strategies can be followed: (i) hybrid material superlattices, which reduce computational time, but also reduce the degrees of freedom for exploring different interface configurations, as the supercell must be built with two perfectly similar A/B and B/A interfaces between materials A and B; or (ii) full hybrid combination of materials with free surfaces. The second solution is the most flexible one, as all the possible interfaces can be analyzed, whatever the crystal orientation and the atomic structure of the interface. This, however, requires heavy DFT calculations and large computational times. In addition, it also requires a good knowledge of the free surface reconstructions and corresponding energies. However, since the knowledge of surface energies is required in any case for the analysis of wetting properties, here, we adopt this second solution for GaP/Si. Figure 1 gives an illustration of a typical supercell used for the calculations. The slab should include the bottom material (that mimics the substrate) with a free surface at the bottom, the top material (that represents the materials deposited on the substrate) with a free surface at the top, and a sufficient thickness of vacuum to avoid any electrostatic charge-charge and dipole-dipole interactions between the slab and its images. The interface is the region between the two different materials. Here, we point out that the implementation of such a method does not require specifying if one given atom belongs to the bulk, to the surface, or to the interface. The only constraint is to fix the positions of some atoms in the middle of the bulk to avoid strain fields that could be induced by the presence of the surrounding free surfaces and the interface.

We define the absolute interface energy ${}^{X}\gamma_{Z}^{Y}$, where X specifies the studied interface, and Y and Z are the top and bottom specific surfaces of the slab related to the two considered materials. The absolute interface energy is thus given by

$$ {}^{X}\gamma_{Z}^{Y} = \frac{E_{\text{slab}}^{\text{int}} - \sum_i \left(N_i \mu_i^{i-\text{bulk}}\right) - \sum_{j=Y,Z} \left(A \gamma_{\text{surf}}^{j}\right)}{A}, \qquad (2) $$

where $E_{\text{slab}}^{\text{int}}$ is the total energy of the slab, $\mu_i^{i-\text{bulk}}$ are the chemical potentials of the N_i atoms composing the material i, γ_{surf}^{j} are the surface energies of surfaces Y and Z (the top and bottom specific surfaces), and A is the in-plane surface area of the slab. Interestingly, Eq. (2) gives an explicit dependency of the interface energy with the chemical potential and the specific surface energies that have been chosen. In our approach, which is shown in Fig. 1, the slab, surfaces, and interface have their own stoichiometries, i.e., their numbers of charges differ from the bulk by a quantity ΔN (difference between the number of P atoms and Ga atoms) referred hereafter as surface or interface stoichiometries. Thus, at the end, the overall deviation to the bulk stoichiometry ΔN for the slab is dependent on the respective stoichiometries of the interface and the two surfaces. Only a careful analysis of the individual stoichiometries allow us to determine absolute surface and interface energies independently. More details about stoichiometry for surface and interface are given in Supplemental Material Sec. 2 [18]. This will be shown hereafter. Furthermore, a specific surface or interface stoichiometry reduced parameter S is defined (Eqs. (S1) and (S2) in the Supplemental Material [18]) as the number of P atoms minus the number of Ga atoms (ΔN) per (1×1) unit cell (a_o^2). This parameter is defined for surface and interface in Supplemental Material Sec. 2 [18].

In the following, we will apply this procedure to the quasilattice-matched GaP/Si model case. While silicon is a homovalent crystal with a diamond structure, GaP and many III-V semiconductors are heterovalent crystals with a zinc-blende structure, which leads to many possible interface atomic configurations.

III. THE GaP/Si ABSOLUTE INTERFACE ENERGY

Calculations were performed within DFT [19,20] as implemented in the SIESTA package [21,22] with a basis set of a finite range of numerical atomic orbitals. Calculations have been carried out with the generalized gradient approximation functional in the PBE form [23] Troullier-Martins pseudopotentials [24], and a basis set of finite-range numerical pseudoatomic orbitals for the valence wave functions [25].

A. Si and GaP surfaces

Although the precise determination of Si and GaP surface energies is first motivated by the absolute interface energy calculation, we provide here a detailed analysis of surface energies for a complete set of stable facets, including the (001) Si and GaP surfaces and higher index (114), (2511), and (111) facets, which have been already observed experimentally for GaP [3,26]. The charge balances for these surfaces were

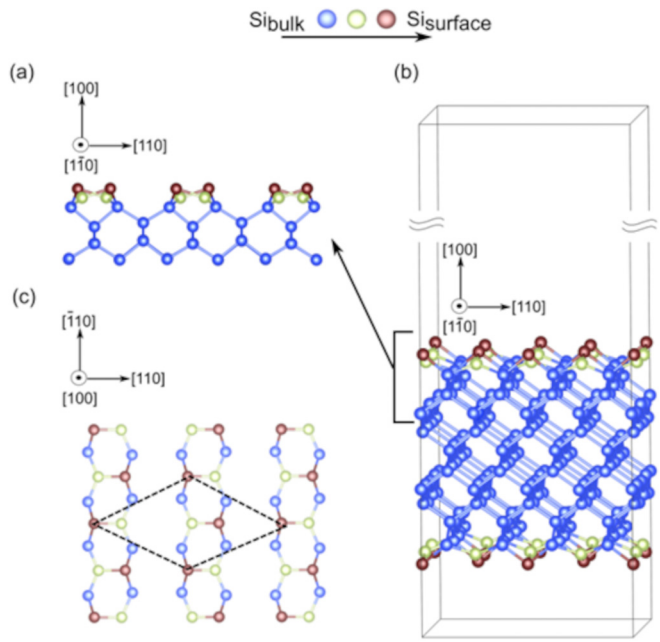

FIG. 2. The Si(001) surface studied by density functional theory (DFT) with (a) side view of the $c(4\times2)$-reconstructed surface, (b) slab with symmetric surfaces realized for DFT calculations, and (c) surface top view with the primitive cell indicated by dashed lines.

carefully analyzed and were found to fulfill the ECM stability criteria [15].

The general equation used to determine the surface energy is

$$\gamma_{\text{surface}} A = E_{\text{slab}} - \sum_i \mu_i N_i, \tag{3}$$

where γ_{surface} is the surface energy, A the surface area, E_{slab} is the slab energy calculated by DFT (after relaxation calculations), μ_i is the chemical potential of the species i, and N_i is the number of particles of the species i in the slab. The temperature dependence is ignored because the contributions tend to cancel for free-energy differences, as claimed for the GaAs material in a previous study [27]. This relation will be upgraded depending on the different surface polarity.

Extensive work has been performed by DFT to study the stability of the different Si surfaces. Among all the stable reconstructions of the flat Si(001) surface, the *minimum minimorum* of surface energy is $c(4\times2)$, where c stands for centered because the dimers are center buckled in a (4×2) configuration [28,29]. To study the surface energy associated with this reconstruction, we built a periodic slab in the [1–10] and [110] directions, whose top surface is orthogonal to the [100] direction. The slab is composed of Si bulk sandwiched between two symmetric surfaces [see Fig. 2(b)]. In the cross-sectional view presented in Fig. 2(a), it is possible to have a better view of the buckling behavior of the dimers, while in Fig. 2(c), the $c(4\times2)$ primitive cell is highlighted by dashed lines in the reconstruction top view.

From the general equation Eq. (3), considering that the top and bottom surfaces have the same surface energies (because it is a nonpolar surface), the silicon surface energy is given by Eq. (4):

$$\gamma_{\text{Si}} = \frac{E_{\text{slab}} - N_{\text{Si}}\mu_{\text{Si-bulk}}}{2A}, \tag{4}$$

where N_{Si} is the total number of Si atoms in the slab. The surface energy of the Si(001) $c(4\times2)$ reconstruction was found to be 92.8 meV/Å^2 and reported in Table I.

For GaP, the different surface and interface energies depend on the chemical potential variations. The chemical potentials μ_{P} and μ_{Ga} are defined as the variables that each element can have within the bulk or surface of the GaP material. The thermodynamic conditions, which the chemical potentials must obey, are the following: the upper limit of μ_{P} and μ_{Ga} is reached when each element is in its own pure bulk phase:

$$\mu_{\text{P}} < \mu_{\text{P}}^{\text{P-bulk}}, \tag{5}$$

$$\mu_{\text{Ga}} < \mu_{\text{Ga}}^{\text{Ga-bulk}}. \tag{6}$$

Moreover, at thermodynamic equilibrium, the sum of μ_{P} and μ_{Ga} must be equal to the chemical potential $\mu_{\text{GaP}}^{\text{GaP-bulk}}$ of the GaP bulk phase:

$$\mu_{\text{Ga}} + \mu_{\text{P}} = \mu_{\text{GaP}}^{\text{GaP-bulk}}, \tag{7}$$

$$\mu_{\text{GaP}}^{\text{GaP-bulk}} = \mu_{\text{Ga}}^{\text{Ga-bulk}} + \mu_{\text{P}}^{\text{P-bulk}} + \Delta H_f(\text{GaP}), \tag{8}$$

where $\Delta H_f(\text{GaP})$ is the heat of formation of GaP material, and $\mu_{\text{P}}^{\text{P-bulk}}$ and $\mu_{\text{Ga}}^{\text{Ga-bulk}}$ are the chemical potentials of the species P and Ga at which the black P and α-Ga phase can form, respectively. In this paper, the value of -0.928 eV for $\Delta H_f(\text{GaP})$ has been determined from the calculated values above, in agreement with the literature [11,14,30].

Here, we therefore calculate the GaP(001), GaP(114), GaP(2511), and GaP(111) surface energies and the GaP/Si interface energy as a function of the phosphorus chemical potential variation $\Delta\mu_{\text{P}} = \mu_{\text{P}} - \mu_{\text{P}}^{\text{P-bulk}}$. Thus, by combining Eqs. (7)–(10), the extreme thermodynamic conditions for $\Delta\mu_{\text{P}}$ are given by

$$\Delta H_f(\text{GaP}) < \Delta\mu_{\text{P}} < 0. \tag{9}$$

Therefore, when $\Delta\mu_{\text{P}}$ equals the heat of formation $\Delta H_f(\text{GaP})$, the extreme Ga-rich limit is reached (i.e., bulk Ga will form preferentially). Contrary to that, when $\Delta\mu_{\text{P}}$ equals 0, the extreme P-rich limit is reached (i.e., bulk P will preferentially form).

For the nonpolar GaP(001) surfaces, the bottom and top surfaces have been treated identically with the same reconstruction which decreases the error on the determination of the surface energy. For the Ga-rich GaP(001) surface, the GaP(001)md (2×4) reconstruction [31,32] (where md stands for mixed dimers) is assumed. This reconstruction is often considered for Ga-rich conditions in the literature [33–35]. For the P-rich GaP(001) (2×4) surface, different stable structures were proposed [36]. In this paper, we studied a simple anion P-rich GaP(001) (2×4) surface that fulfills the ECM criteria as proposed for GaAs [15]. The thicknesses of the slabs are $\sim$ 17 and 23 Å, respectively, for the P-rich GaP(001) (2×4) surface [Figs. 3(a) and 3(c)] and for the Ga-rich GaP(001)md (2×4) surface [Figs. 3(d) and 3(f)]. The outermost atoms (within $\sim$ 6 Å from the vacuum region) of the top and bottom surfaces were allowed to relax to their minimum

TABLE I. Stable GaP and Si surface energies computed by DFT and corresponding surface stoichiometries. The surface stoichiometry parameters S_{surf} per (1×1) unit cell of GaP (a^2_{GaP}). The in-plane surface area A of these slabs per (1×1) unit cell of GaP.

Surface	A/a^2_{GaP}	ΔN_{surf}	S_{surf}	Energy (meV/Å^2)	
				P-rich	Ga-rich
Si(001) $c(2\times4)$				92.8	
GaP(001) (2×4)	8	4	$\frac{1}{2}$	57.4	72.4
GaP(001)md (2×4)	8	−8	−1	82.8	52.9
GaP(114)*B*-α2(2×1)	$3\sqrt{2}$	0	0	67.3	67.3
GaP(114)*A*-α2(2×1)	$3\sqrt{2}$	0	0	59.9	59.9
GaP(2511)*B*-(1×1)-Ga-dimer	$\frac{5\sqrt{7}}{2}\cos(22.21)$	+2	$\frac{1}{\sqrt{150}}$	66.8	58.3
GaP(2511)*A*-(1×1)-P-dimer	$\frac{5\sqrt{7}}{2}\cos(22.21)$	−2	$-\frac{1}{\sqrt{150}}$	52.9	62.7
GaP(111)*A*-Ideal	$2\sqrt{3}$	−2	$-\frac{1}{\sqrt{3}}$	95.7	78.4
GaP(111)*B*-Ideal	$2\sqrt{3}$	+2	$\frac{1}{\sqrt{3}}$	75.1	92.3
GaP(111)*A*-Ga-vacancy	$2\sqrt{3}$	0	0	51.2	51.2
GaP(111)*B*-Ga-adatom	$2\sqrt{3}$	0	0	57.3	57.3
GaP(111)*A*-Ga-trimer	$2\sqrt{3}$	−8	$-\frac{4}{\sqrt{3}}$	106.4	37.3
GaP(111)*B*-P-trimer	$2\sqrt{3}$	+8	$\frac{4}{\sqrt{3}}$	20.2	89.3

energy configuration, and all other atoms were kept frozen in the bulk position.

The strategy used for the silicon surface is still pertinent for nonpolar GaP(001), as top and bottom surfaces are the same. For this nonpolar surface, again, the energy of one surface is half the total energy of the back and top surfaces. However, in this case, both the chemical potential and the stoichiometry have an impact on the surface energy variations. The surface energy is thus expressed as

$$\gamma_{\text{GaP(001)}} = \frac{E_{\text{slab}} - N_{\text{Ga}}\mu_{\text{GaP}}^{\text{GaP-bulk}} - (N_{\text{P}} - N_{\text{Ga}})\mu_{\text{P}}}{2A}, \quad (10)$$

where N_{Ga} and N_{P} are, respectively, the numbers of Ga and P atoms in the slab. The deviation of the surface stoichiometry as compared with the one of the bulk $\Delta N_{\text{surface}}$ is reported in Table I. Surface energies are found equal to 72.4 (52.9) meV/Å^2 in Ga-rich conditions and 57.4(82.8) meV/Å^2 in P-rich conditions for the GaP(001) (2×4) surface [for the GaP(001)md (2×4) surface].

For polar (114), (2511), and (111) surfaces, the previous simple approach cannot be adopted because top and bottom surfaces are different. Type *A* and *B* polar surfaces [37] were computed for each investigated surface. Letter *A*(*B*) refers to P(Ga)-terminated surfaces. Consequently, a different approach has been applied for these cases. It consists of considering the top surface as the one being investigated and passivating the bottom one with fictitious hydrogen atoms (see Supplemental Material Sec. III [18]). The method and its validity are discussed in Supplemental Material Sec. IV [18].

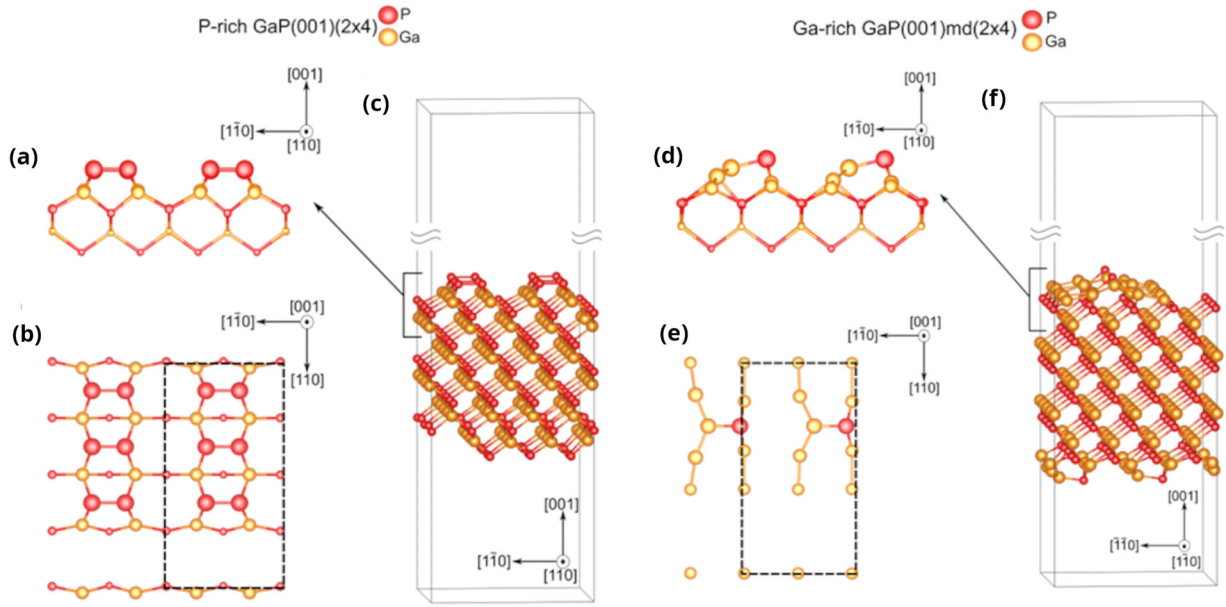

FIG. 3. (a) Side profile, (b) top view, and (c) the slab realized for P-rich GaP(001) (2×4) surface. (d) Side profile, (e) top view, and (f) the slab realized for Ga-rich GaP(001) (2×4)md surface. Dashed lines in the top views indicate the unit cells of the reconstructions.

Thus, surface energies are found equal to 67.3meV/Å^2 for the P-rich GaP(114)*B*-α2(2×1) (Figs. S4(a)–S4(c) in the Supplemental Material [18]), and 59.9 meV/Å^2 for the Ga-rich GaP(114)*A*-α2(2×1) (Figs. S4(d)–S4(f) in the Supplemental Material [18]). With such stoichiometric surfaces, $N_P = N_{Ga}$, and therefore, the values found apply for the whole range of chemical potentials. These results are reported in Table I.

With the same procedure, other stable facets can be considered. Different authors (e.g., for GaAs or GaP-based materials) have reported on the observation of III-V crystal facets lying around the (136) orientation in the stereographic triangle [3,38–42]. The need to fulfill the ECM stability criteria led to the identification of the (2511) plane as the most stable facet at the vicinity of the (136) orientation [38–40]. The two reconstructions are named, respectively, P-dimer GaP(2511)$A-(1\times1)$, as shown in Figs. S5(a)–S5(c) in the Supplemental Material [18], and Ga-dimer GaP(2511)$B-(1\times1)$, as shown in Figs. S5(d)–S5(f) in the Supplemental Material [18] (we use the notation of Refs. [38,39]). The polar surface reconstructions were passivated by the fictitious H* with fractionally charged hydrogen 1.25*e* and 0.75*e* for Ga and P dangling bonds. Then the subsurfaces opposite to the passivated surface of the slab were allowed to relax ~ 6 Å into their minimum energy, and all the other atoms were kept frozen in the bulk position except the fictitious H* atoms which were also allowed to relax. Like the (114) facet case, Eq. (S5) in the Supplemental Material [18] is used to calculate the surface energy of the two different *A* and *B* (2511) facets. Surface energies are found equal to 62.7 (58.3) meV/Å^2 in Ga-rich conditions and 52.9 (66.8) meV/Å^2 in P-rich conditions for the P-dimer GaP(2511)$A-(1\times1)$ surface [Ga-dimer GaP(2511)$B-(1\times1)$]. Unlike the (114) surfaces, these reconstructions are not stoichiometric, and therefore, the surface energies vary with the phosphorus chemical potential. Results are summarized in Table I.

Finally, additional calculations were performed on various GaP(111) surfaces. The (111) facets are commonly identified in several works [27,37,43–55]. We first considered the two ideal surfaces, namely, GaP(111)*A*-ideal and GaP(111)*B*-ideal. These surface energies are found equal to 78.4 (92.3) meV/Å^2 in Ga-rich conditions and 95.7 (75.1) meV/Å^2 in P-rich conditions for the GaP(111)*A*-ideal surface [GaP(111)*B*-ideal]. Then we studied the two surfaces which are respecting the ECM by adding or removing a Ga atom, namely, GaP(111)*A*-Ga-vacancy, as shown in Figs. S6(a)–S6(c) in the Supplemental Material [18], and GaP(111)*B*-Ga-adatom, as shown in Figs. S6(d)–S6(f) in the Supplemental Material [18]. Here, $N_P = N_{Ga}$; therefore, the values of the surface energy are not evolving with the chemical potential. Surface energies are found equal to 51.2 meV/Å^2 for the P-rich GaP(111)*A*-Ga-vacancy and 57.3 meV/Å^2 for the Ga-rich GaP(111)*B*-Ga-adatom. In addition, the two extreme cases where trimers of Ga or P are forming on the surface, namely, GaP(111)*A*-Ga-trimer, as shown in Figs. S7(a)–S7(c) in the Supplemental Material [18], and GaP(111)*B*-P-trimer, as shown in Figs. S7(d)–S7(f) in the Supplemental Material [18], are also considered in this paper. These surface energies are found equal to 37.3 (89.3) meV/Å^2 in Ga-rich conditions and 106.4 (20.2) meV/Å^2 in P-rich conditions for the GaP(111)*A*-Ga-trimer surface [GaP(111)*B*-P-trimer].

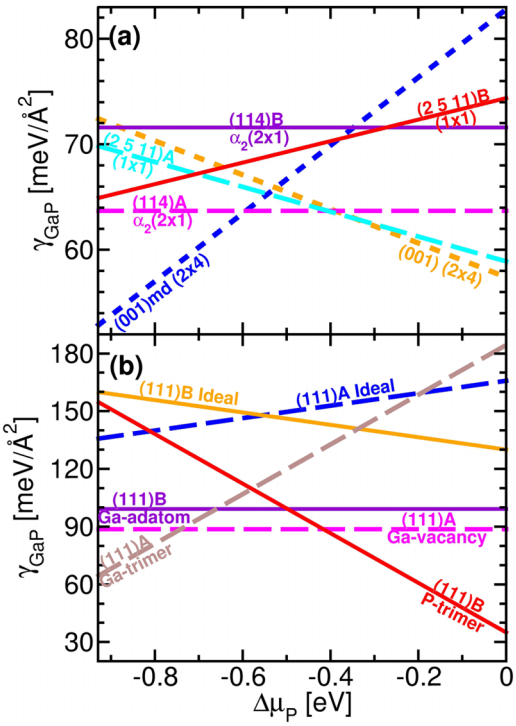

FIG. 4. Absolute surface energies of various GaP stable surfaces as a function of the chemical potential variations for (a) (001), (114), and (2511) GaP surfaces and (b) (111) GaP surfaces. All the surface energies have been corrected from their angle θ to compare their stability on a (001) substrate.

Overall, all the previously calculated surface energies are summarized in Table I. Experimentally, the growth is imposed on the specific direction (001). The appearance of other facets may result from the competition between surface energy of the (001) surface and surface energies of other stable surfaces. In fact, the possible destabilization of the (001) surface by other surfaces on a (001) substrate can be easily calculated after the pioneering works of Poynting and Thompson [56] and others' studies [26,57]. Consequently, one should consider the corrected surface energy:

$$\gamma_{U/001} = \frac{\gamma_U}{\cos(\theta)}, \tag{11}$$

where $\gamma_{U/001}$ is the corrected surface energy of the considered stable facet *U*, growing on a (001) substrate. In our case, *U* is the studied surface (114), (2511), or (111), and θ is the angle between *U* and the (001) surfaces. Here, the related angles are 19.47°, 26.09°, and 54.74° for (114), (2511), and (111) surfaces, respectively. Thus, the surface energies (114), (2511), and (111) are divided by [Eq. (11)] 0.94, 0.90, and 0.58, respectively. Figure 4 shows the corrected surface energies as a function of the variation of the chemical potential P. From Ga-rich to P-rich, the most stable surfaces are GaP(001)md (2×4) for the extreme case of Ga-rich, GaP(114)*A*-α2(2×1) in the middle, and GaP(001) (2×4) in

TABLE II. Calculated dimer lengths, in units of Å, of the surface atoms for the P-rich GaP(001) (2×4), Ga-rich GaP(001)md (2×4), GaP(114)*B*-α2(2×1), GaP(114)*A*-α2(2×1), GaP(2511)$B-(1\times1)$, GaP(2511)$A-(1\times1)$, and GaP(111)*A* and *B* reconstructions. Dimer lengths of black phosphorus, α-Ga phase, and GaP are also reported.

	Dimer length	
Surface reconstruction and bulk materials	P-P	Ga-Ga
P-rich GaP(001) (2×4)	2.30 ± 0.01	
P-rich GaP(114)*B*-α2(2×1)	2.32 ± 0.02	2.58 ± 0.06
Ga-rich GaP(114)*A*-α2(2×1)	2.30 ± 0.01	2.77 ± 0.01
GaP(2511)*B*-(1×1)-Ga-dimer		2.54 ± 0.07
GaP(2511)*A*-(1×1)-P-dimer	2.30 ± 0.01	
GaP(111)*A*-Ga-trimer		2.74 ± 0.20
GaP(111)*B*-P-trimer	2.32 ± 0.01	
Black phosphorus	2.28 ± 0.01	
α-Ga phase		2.83 ± 0.07
	md Ga-P	
Ga-rich GaP(001)md (2×4)	2.41 ± 0.02	
GaP	2.41 ± 0.01	

competition with GaP(2511)$A-(1\times1)$ for the extreme case of P-rich. In addition, GaP(111)*B*-P-trimer is even more stable than GaP(001) (2×4) and GaP(2511)$A-(1\times1)$ but only in the P-rich limit.

The reconstruction of studied surfaces shows a diversity of arrangement of dimers, as displayed in Figs. 3 and S4–S7 in the Supplemental Material [18], and dimer lengths are also reported in Table II. The mixed dimers of Ga-P, as in Figs. 3(d)–3(f), for the Ga-rich GaP(001)md (2×4) surface, are found to have a characteristic length of 2.41 Å, which is also the same value as the typical distance between Ga and P atoms in the bulk material. The phosphorus dimers (in Figs. 3(a)–3(c), S4, S5(a)–S5(c), and S7(d)–S7(f) in the Supplemental Material [18]) have similar lengths for P-rich GaP(001) (2×4), GaP(114)*A* and *B*, GaP(2511)$A-(1\times1)$, and GaP(111)*B*-P-trimer surfaces. The phosphorus dimer lengths for all of these surface reconstructions are nearly the same as black phosphorus material. Instead, the gallium

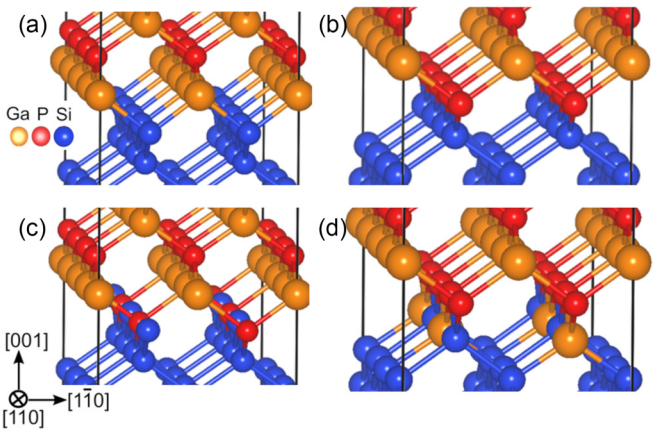

FIG. 5. Zoomed atomic configuration for the two abrupt interfaces (a) Si-Ga, (b) Si-P, and the two compensated interfaces (c) 0.5Si:0.5P-Ga, (d) 0.5Si:0.5Ga-P, respectively.

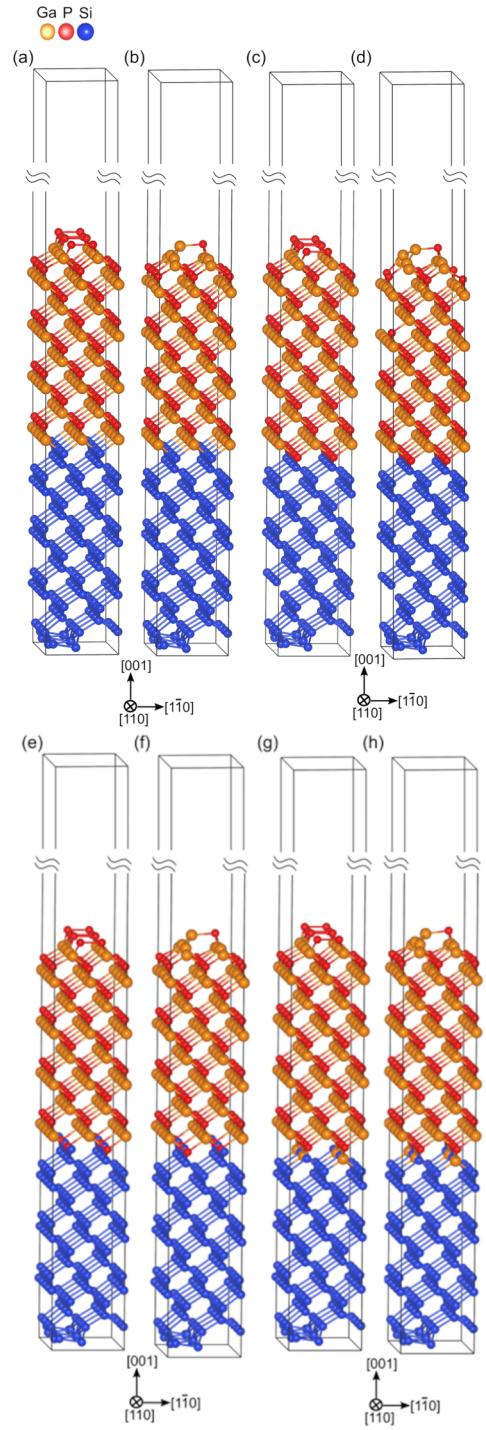

FIG. 6. On the top, schematic of the four slabs used in density functional theory (DFT) for the calculation of the absolute interface energy of the abrupt Ga-Si interface with (a) P-rich GaP(001) (2×4) and (b) Ga-rich GaP(001)md (2×4) surfaces reconstructions and of the abrupt P-Si interface with (c) P-rich GaP(001) (2×4) and (d) Ga-rich GaP(001)md (2×4) surfaces reconstructions. On the bottom, four slabs used in DFT for the calculation of the absolute interface energy of the Ga-Si interface compensated with P named 0.5Si:0.5P-Ga interface with (e) P-rich GaP(001) (2×4) and (f) Ga-rich GaP(001)md (2×4) surface reconstructions and the P-Si interface compensated with Ga named 0.5Si:0.5Ga-P interface with (g) P-rich GaP(001) (2×4) and (h) Ga-rich GaP(001)md (2×4) surface reconstructions.

dimer lengths (Figs. S4, S5(d)–S5(f), and S7(a)–S7(c) in the Supplemental Material [18]) are much more different, and we can separate them in two categories: the shorter bond lengths for the GaP(114)*B*-α2(2×1) and GaP(2511)*A* − (1×1) cases and the larger bond lengths for the GaP(114)*A*-α2(2×1) and GaP(111)*A*-Ga-trimer cases. The variation between the two categories is ~ 0.2 Å. In fact, the gallium dimer lengths of the Ga-rich GaP(114)*A*-α2(2×1) and GaP(111)*A*-Ga-trimer surfaces tend to be like the α-Ga phase. Finally, this simple analysis tends to reveal that the elastic energy should decrease for the polar surface (114)*A* because Ga-Ga and P-P dimer lengths are quite comparable with their length within bulk materials such as α-Ga phase and black phosphorus. Similarly, for the (2511)*A* and *B* surfaces, the surface energy decreases (increases) for the polar surface *A*(*B*) because there is less (more) difference than the dimer length within bulk materials such as black phosphorus (α-Ga phase). Identically, we have the same conclusion for the polar surfaces GaP(111)*A*-Ga-trimer and GaP(111)*B*-P-trimer, where the GaP(111)*B*-P-trimer is more stable, also due to elastic energy which decreases as the bond lengths of the dimers are closer to bulk black phosphorus.

B. GaP/Si interfaces

The thermodynamic analysis of the GaSiP phases indicates a broad stability region shaded in blue (see Figs. S8 and S9 in the Supplemental Material [18]) for the GaP/Si interface. Indeed, only two secondary phases SiP and Si_2 for extreme Ga-poor and Si-rich growth conditions are in competition with the GaP/Si interface. Otherwise, GaP/Si interfaces are expected to be stable, with no secondary phase. The GaP-Si heterointerface energy has already been investigated by previous works. Indeed, results on the relative interface formation energy of GaP on different Si surfaces has already been presented in Ref. [14]. The stability of the compensated GaP/Si(001) interface with respect to an abrupt one has been reported as well in Refs. [11,12] by calculating its relative formation energy. The GaP/Si(001) absolute abrupt interface energy has also been determined [13], but these results have been questioned in Ref. [58] since the dependence from the chemical potential of the absolute interface energy has not been considered. Finally, a correct determination of the different GaP/Si(001) absolute interface energies has not yet been proposed.

Our DFT calculations to determine the GaP/Si(001) absolute interface energies as a function of the chemical potential are presented in the following. The calculations computed by DFT have been done using the same parameters already reported in the paragraph above for the GaP surface energies study.

To determine the interface energies, we studied first the abrupt P/Si and Ga/Si interfaces [Figs. 5(a) and 5(b)] and then the nonabrupt [12], also called compensated, 0.5Si:0.5Ga-P and 0.5Si:0.5P-Ga interfaces [Figs. 5(c) and 5(d)]. For the abrupt interfaces, the slabs are shown in Figs. 6(a)–6(d). In fact, for each interface, two different top surfaces are modeled to check the validity of the results and confirm that interface energies and their variations with chemical potential are independent of the top surface. Therefore, the two reconstructed GaP(001) surfaces were used for this purpose: Ga-rich GaP(001)md (2×4) and P-rich GaP(001) (2×4). The unit cell of each one is shown in the top view section in Fig. 3. Note that, instead of keeping reconstructed GaP top surfaces and Si bottom surfaces, for the absolute interfacial energy determination, one could prefer using GaP and Si surfaces passivated with fictitious hydrogen atoms to avoid parasitic surface/surface or surface/interface interactions. This approach is meaningful but needs a precise evaluation of the contributions of passivated surfaces to the total energy of the slab. In this paper, the large vacuum thickness, the large material thickness, and the systematic comparison of the interface energies for two very different GaP surfaces guarantee the weak contribution of these parasitic interactions. The stoichiometry of the interface for a slab is provided by the relation below:

$$\Delta N_{\text{int}} = \Delta N_{\text{slab}} - \Delta N^{\text{Top}}_{\text{surface}} - \Delta N^{\text{Bottom}}_{\text{surface}}, \tag{12}$$

where ΔN_{slab}, $\Delta N^{\text{Top}}_{\text{surface}}$, and $\Delta N^{\text{Bottom}}_{\text{surface}}$ are the stoichiometry of the entire slab, the GaP surface at the top, and the silicon surface at the bottom, respectively. Here, the stoichiometry of the silicon surface at the bottom is equal to 0, $\Delta N^{\text{Bottom}}_{\text{surface}} = 0$, which reduces Eq. (12). For the abrupt interfaces, the ECM is not respected (stoichiometry of +4 or −4), as shown in Table III, whereas for the compensated interfaces, the ECM is respected (stoichiometry equals 0).

The slabs are separated by a vacuum region of 450 Å thick. To avoid any surface/interface interaction, both GaP and Si bulk are 20 Å thick each. More precisely, the slab lengths in Figs. 6(a), 6(e) and 6(b), 6(f) are, respectively, 42.31 and 43.62 Å, while the slabs in Figs. 6(c), 6(g) and 6(d), 6(h) have, respectively, lengths of 40.9 and 45 Å. For each slab, the basis vector lengths are 15.44 and 7.72 Å. We choose Si(001) as the bottom surface for each case investigated. Finally, the entire GaP together with the two first layers of silicon at the interface was allowed to relax, while the rest was frozen.

The absolute interface energy ${}^{X}\gamma^{Y}_{Z}$ is finally calculated using Eq. (2) applied to the present specific case:

$${}^{X}\gamma^{Y}_{Z} = \frac{E^{\text{int}}_{\text{slab}} - N_{\text{Ga}}\mu^{\text{GaP-bulk}}_{\text{GaP}} - (N_{\text{P}} - N_{\text{Ga}})\mu_{\text{P}} - N_{\text{Si}}\mu^{\text{Si-bulk}}_{\text{Si}} - A\gamma^{\text{Si}}_{\text{surf}} - A\gamma^{\text{GaP}}_{\text{surf}}}{A}, \tag{13}$$

where $E^{\text{int}}_{\text{slab}}$ is the total energy of the slab, N_{Ga} and N_{P} are, respectively, the number of Ga and P atoms of the slab investigated, $\mu^{\text{GaP-bulk}}_{\text{GaP}}$ and μ_{P} are the chemical potentials of the GaP bulk and species P, *A* is the rectangular base surface area, $\mu^{\text{Si-bulk}}_{\text{Si}}$ is the chemical potential of the silicon bulk, while N_{Si} is the number of silicon atoms, and $\gamma^{\text{Si}}_{\text{surf}}$ and $\gamma^{\text{GaP}}_{\text{surf}}$ are the

TABLE III. Stoichiometry of abrupt and compensated interfaces under different surfaces, ΔN_{int}. Stoichiometry of the slab and of the top surface, ΔN_{slab} and $\Delta N^{\text{Top}}_{\text{surface}}$. The interface stoichiometry parameters per (1×1) unit cell of Si (a_o^2). The in-plane surface area A of these slabs is $4a_o^2$.

Slab configuration	Interface	Bottom surface	Top surface	ΔN_{slab}	$\Delta N^{\text{Top}}_{\text{surface}}$	ΔN_{int}	S_{int}
$^{\text{Si-Ga}}\gamma^{\text{Si(100)}}_{\text{GaP(001)2}\times4}$	Si-Ga	Si (100)	GaP (001) 2×4	-2	2	-4	-1
$^{\text{Si-Ga}}\gamma^{\text{Si(100)}}_{\text{GaP(001)2}\times4\text{md}}$	–	–	GaP (001) 2×4md	-8	-4	-4	-1
$^{\text{Si-P}}\gamma^{\text{Si(100)}}_{\text{GaP(001)2}\times4}$	Si-P	–	GaP (001) 2×4	6	2	4	1
$^{\text{Si-P}}\gamma^{\text{Si(100)}}_{\text{GaP(001)2}\times4\text{md}}$	–	–	GaP (001) 2×4md	0	-4	4	1
$^{\text{0.5Si:0.5P-Ga}}\gamma^{\text{Si(100)}}_{\text{GaP(001)2}\times4}$	0.5Si:0.5P-Ga	–	GaP (001) 2×4	2	2	0	0
$^{\text{0.5Si:0.5P-Ga}}\gamma^{\text{Si(100)}}_{\text{GaP(001)2}\times4\text{md}}$	–	–	GaP (001) 2×4md	-4	-4	0	0
$^{\text{0.5Si:0.5Ga-P}}\gamma^{\text{Si(100)}}_{\text{GaP(001)2}\times4}$	0.5Si:0.5Ga-P	–	GaP (001) 2×4	2	2	0	0
$^{\text{0.5Si:0.5Ga-P}}\gamma^{\text{Si(100)}}_{\text{GaP(001)2}\times4\text{md}}$	–	–	GaP (001) 2×4md	-4	-4	0	0

specific bottom and top surface energies per unit area. For interfaces, the chemical potential of species P varies in the same interval range as the GaP surface case.

The results are reported in Table IV. The Si-Ga interface is always more stable in a Ga-rich environment, while the Si-P interface is more stable in a P-rich one. Moreover, as expected, this is independent of the kind of surface considered within a small numerical error. Finally, the absolute variation of the interface energy from P-rich to Ga-rich conditions is always of 31.2 meV/Å^2 for Si-Ga and Si-P interfaces, respectively, in agreement with the inverse stoichiometry of both interfaces. Finally, the averages of stable GaP and Si absolute interface energies computed by DFT from Table IV are shown in Table V and are plotted as a function of the chemical potential in Fig. 7. The lowest value is reached (23.4 meV/Å^2) with a III-V/Si Ga-compensated interface. The same evolution as the one presented in Ref. [12] with relative comparisons between interfaces is observed, with an overall better stability of compensated interfaces over the whole range of chemical potentials. It is also worth mentioning that the formation of the compensated interface drastically changes the absolute value of the interface energy. For instance, in Ga-rich conditions, the interface energy is divided by 2 as compared with the abrupt Ga-Si interface case. Therefore, the compensated interfaces are more likely to form during GaP/Si epitaxy and in general during III-V/Si epitaxy. We note here that the interface energies of the most stable interfaces computed in this paper (between 20 and 30 meV/Å^2) appear much lower than the one experimentally inferred by Ponchet *et al.* [59] that was estimated in the range of $[55-110]$ meV/Å^2 for III-Sb/Si. While the change of materials system alone can hardly explain such a difference, this result raises questions about the influence of the passivation of the starting Si surface prior to the growth on the surface energy, which will be discussed later on in this paper, and the contribution of interfacial defects to the interface energy, which was discussed in detail in Ref. [59]. Overall, the good stability of III-V/Si interfaces may significantly change the wetting properties of the system. Therefore, in the following, we examine the influence of the interface structure on the wetting properties for the GaP/Si model case.

IV. GaP/Si WETTING PROPERTIES

To investigate the wetting properties for the GaP/Si case, the surface and interface energies computed can be used to determine the Young-Dupré spreading parameter Ω [17]. A positive value of Ω corresponds to perfect wetting conditions, while a negative value corresponds to partial wetting, i.e., a Volmer-Weber growth, or perfect nonwetting conditions, leading to the formation of three-dimensional (3D) islands whose equilibrium shape depends on Ω [59–62]. Figure 8 represents

TABLE IV. GaP/Si absolute interface energies computed by DFT.

				Energy (meV/Å^2)	
Slab configuration	Interface	Bottom surface	Top surface	P-rich	Ga-rich
$^{\text{Si-Ga}}\gamma^{\text{Si(100)}}_{\text{GaP(001)2}\times4}$	Si-Ga	Si (100)	GaP (001) 2×4	72.0	40.8
$^{\text{Si-Ga}}\gamma^{\text{Si(100)}}_{\text{GaP(001)2}\times4\text{md}}$	–	–	GaP (001) 2×4md	69.7	38.5
$^{\text{Si-P}}\gamma^{\text{Si(100)}}_{\text{GaP(001)2}\times4}$	Si-P	–	GaP (001) 2×4	25.9	57.1
$^{\text{Si-P}}\gamma^{\text{Si(001)}}_{\text{GaP(001)2}\times4\text{md}}$	–	–	GaP (001) 2×4md	27.3	58.4
$^{\text{0.5Si:0.5P-Ga}}\gamma^{\text{Si(100)}}_{\text{GaP(001)2}\times4}$	0.5Si:0.5P-Ga	–	GaP (001) 2×4	28.3	28.3
$^{\text{0.5Si:0.5P-Ga}}\gamma^{\text{Si(100)}}_{\text{GaP(001)2}\times4\text{md}}$	–	–	GaP (001) 2×4md	26.2	26.2
$^{\text{0.5Si:0.5Ga-P}}\gamma^{\text{Si(100)}}_{\text{GaP(001)2}\times4}$	0.5Si:0.5Ga-P	–	GaP (001) 2×4	24.7	24.7
$^{\text{0.5Si:0.5Ga-P}}\gamma^{\text{Si(100)}}_{\text{GaP(001)2}\times4\text{md}}$	–	–	GaP (001) 2×4md	22.1	22.1

TABLE V. Average values for stable GaP/Si absolute interface energies computed by DFT from the Table IV.

Slab configuration	Interface	Bottom surface	Top surface	Energy (meV/Å^2)	
				P-rich	Ga-rich
$^{Si-Ga}\gamma^{Si(100)}_{GaP(001)}$	Si-Ga	Si (100)	GaP (001)	70.9	39.7
$^{Si-P}\gamma^{Si(100)}_{GaP(001)}$	Si-P	–	–	26.6	57.8
$^{0.5Si:0.5P-Ga}\gamma^{Si(100)}_{GaP(001)}$	0.5Si:0.5P-Ga	–	–	27.3	27.3
$^{0.5Si:0.5Ga-P}\gamma^{Si(100)}_{GaP(001)}$	0.5Si:0.5Ga-P	–	–	23.4	23.4

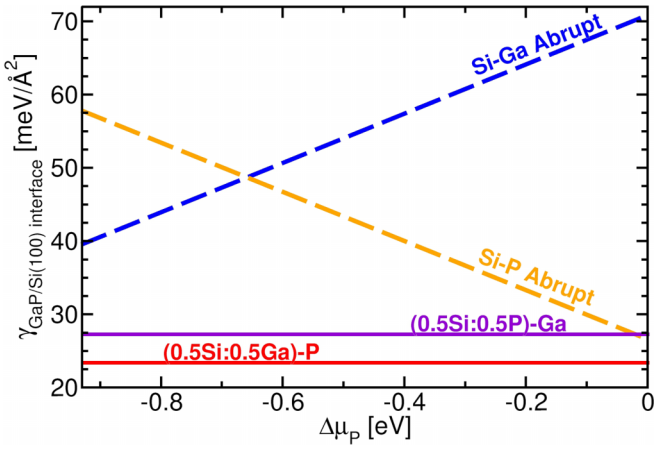

FIG. 7. Average absolute interface energies diagram of both compensated and abrupt interfaces computed by density functional theory (DFT). As reported in Ref. [12], the compensated 0.5Si:0.5Ga-P and 0.5Si:0.5P-Ga energies are more stable with respect to the abrupt ones because they fulfill the electron counting model (ECM) criterion. Moreover, their energy does not vary with the chemical potential $\Delta\mu_P$ as expected because of their stoichiometry ($\Delta N = 0$).

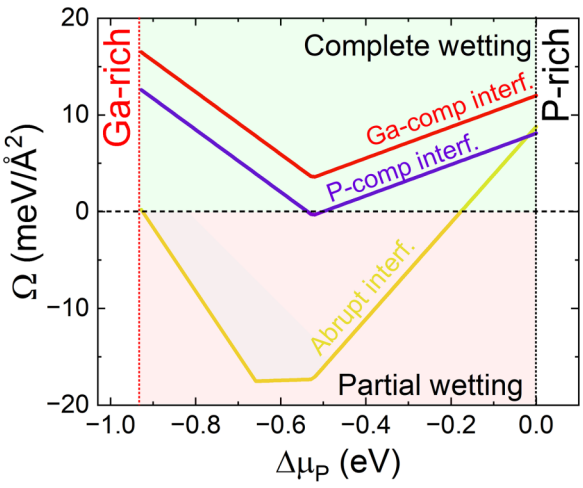

FIG. 8. Young-Dupré spreading parameter Ω as a function of the chemical potential $\Delta\mu_P$, calculated for the different interface atomic configurations: (i) Abrupt III-V/Si interfaces (orange), (ii) P-compensated III-V/Si interface (purple), and (iii) Ga-compensated III-V/Si interface (red).

the calculated values of Ω for the same GaP and Si surface energies but with different interfacial atomic configurations.

In this calculation, $\gamma^S_{(Si)}$ is kept constant at 92.8 meV/Å^2, and $\gamma^S_{(III-V)}$ is taken as the lowest GaP(001) surface energy (most stable surface) for a given chemical potential. Thus, for $\Delta\mu_P > -0.52$ eV, the P-rich GaP(001) (2×4) was chosen, while for $\Delta\mu_P < -0.52$ eV, the Ga-rich GaP(001)md (2×4) was alternately considered, explaining the systematic slope change at $\Delta\mu_P = -0.52$ eV observed in Fig. 8. With this approach, the spreading parameter Ω is first calculated in the case where abrupt Ga-Si or P-Si interfaces are considered (orange solid line in Fig. 8). In this case, unlike what was done in previous work [3], the most stable interface configuration for a given chemical potential was considered. Thus, for $\Delta\mu_P < -0.65$ eV, the Ga-Si abrupt interface was chosen, while for $\Delta\mu_P > -0.65$ eV, the P-Si abrupt interface was considered. This, again, leads to a slope variation at $\Delta\mu_P = -0.65$ eV for Ω. According to Fig. 8, Ω remains negative throughout most of the $\Delta\mu_P$ chemical potential range, which means that partial wetting is very likely to be achieved. The same calculation was thus performed with the most stable interface atomic configurations, corresponding to situations where the interface is either compensated by P (P-compensated III-V/Si interfaces, purple solid line in Fig. 8) or by Ga (Ga-compensated III-V/Si interfaces, red solid line in Fig. 8). In these two cases, the interface energy does not depend on the chemical potential, and Ω remains positive for all values of chemical potential, leading to predicted complete wetting conditions. This result is theoretically not surprising, as it is a direct consequence of Eq. (1). A lower interface energy means a lower energy cost to form a 2D layer on the substrate, thus favoring the complete wetting of the material on the substrate. On the other hand, it apparently contradicts recent experimental work, in which authors demonstrated that III-V/Si epitaxial growth happens under partial wetting conditions [3,7]. As explained previously, the wetting conditions are fully determined by the sign of Ω. The extended studies conducted in this paper allow us to conclude that, overall, III-V (001) surface energies lie in the $[50-70]$ meV/Å^2 range and that the III-V/Si interfaces are compensated, with energies in the [20–30] meV/Å^2 range. However, in this paper, a nude Si(001) surface was assumed to be representative of the substrate surface before the III-V epitaxy. As discussed in previous work [3], the nude Si surface is very reactive because of its high surface energy and will thus tend to passivate by creating bonds with other atoms available at the surface during chemical preparation (e.g., H, O) or annealing prior to epitaxial growth (e.g., As, P, Sb, Ga, In, Al, N). In the

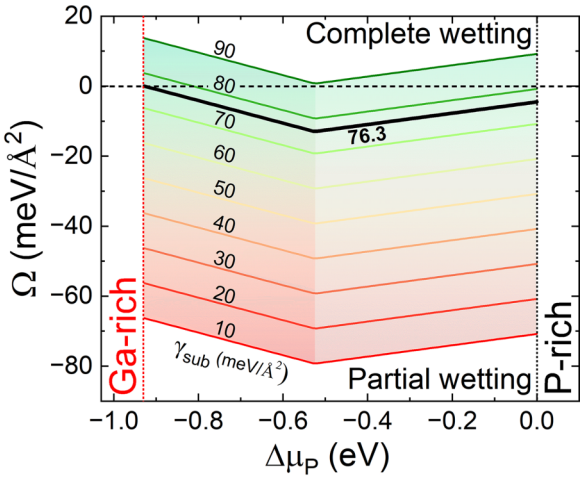

FIG. 9. Young-Dupré spreading parameter Ω as a function of the chemical potential $\Delta\mu_P$, calculated for different substrate surface energies [from 10 meV/Å^2 (red) to 90 meV/Å^2 (green)], with the most stable Ga-compensated III-V/Si interface.

following, we investigate quantitatively the contribution of the substrate surface energy to the wetting properties.

Figure 9 represents the calculated values of Ω for the most stable GaP surfaces and GaP-Si interfaces (i.e., with a Ga-compensated III-V/Si interface), for different values of the substrate surface energy γ^S_{sub}, ranging from 10 meV/Å^2 (red solid line) to 90 meV/Å^2 (green solid line). Here, Ω is always positive for substrate surface energies > 90 meV/Å^2. On the other hand, Ω rapidly evolves toward negative values, even for small variations of the substrate surface energy, rapidly leading to partial wetting conditions. For a substrate surface energy of 76.3 meV/Å^2, Ω is already negative for the whole range of chemical potentials. This means that any energy gain through stabilization of the starting Si surface by >16.5 meV/Å^2 is enough to promote partial wetting conditions (i.e., growth of 3D islands). Even with an ultrapure Si surface cleaning procedure and assuming that the epitaxial chamber is free of unintentional contaminants that could incorporate at the surface, the simple exposure of the Si surface to a group-V atom flux at the beginning of the growth may easily stabilize the Si surface at lower values, leading to partial wetting conditions. While this analysis focused on the GaP/Si case, ranges for surface and interface energies are expected to remain the same for other III-V/Si material systems. For this reason, even if similar studies could be conducted for other III-V materials and considering the specific surface energies of various passivated Si surfaces, the complete wetting of a Si substrate by a 2D III-V semiconductor layer appears unlikely. The detailed analysis of the Si surface passivation is consequently of great importance for the complete understanding of the system.

V. CONCLUSIONS

In conclusion, absolute surface and interface energies were calculated for various atomic configurations of GaP surfaces and GaP/Si (001) interfaces by using DFT. These studies not only confirm the large stability of compensated III-V/Si interfaces but allow a quantitative analysis of the different surface and interface contributions to the wetting properties of the material system. The large stabilization of the III-V/Si interface through charge compensation is expected to promote the complete wetting conditions in the system. We show that this effect is, however, easily counterbalanced by the pregrowth passivation (intentional or not) of the Si substrate surface. This quantitative analysis confirms that the complete analysis of wetting properties of III-V semiconductors on Si surfaces appears strongly dependent on the passivation of the initial Si surface, which drastically impacts the spreading parameter.

ACKNOWLEDGMENTS

This paper was supported by the French National Research (Agence Nationale de la Recherche, FRANCE) NUAGES Project (Grant No. ANR-21-CE24-0006). DFT calculations were performed at FOTON Institute, and we were granted access to the HPC resources of TGCC/CINES under Allocation No. A0120911434 made by GENCI.

[1] G. Saint-Girons, J. Cheng, P. Regreny, L. Largeau, G. Patriarche, and G. Hollinger, Accommodation at the interface of highly dissimilar semiconductor/oxide epitaxial systems, Phys. Rev. B **80**, 155308 (2009).

[2] G. Niu, G. Saint-Girons, B. Vilquin, G. Delhaye, J.-L. Maurice, C. Botella, Y. Robach, and G. Hollinger, Molecular beam epitaxy of $SrTiO_3$ on Si (001): Early stages of the growth and strain relaxation, Appl. Phys. Lett. **95**, 062902 (2009).

[3] I. Lucci, S. Charbonnier, L. Pedesseau, M. Vallet, L. Cerutti, J.-B. Rodriguez, E. Tournié, R. Bernard, A. Létoublon, N. Bertru *et al.*, Universal description of III-V/Si epitaxial growth processes, Phys. Rev. Mater. **2**, 060401(R) (2018).

[4] N. H. Karam, R. R. King, M. Haddad, J. H. Ermer, H. Yoon, H. L. Cotal, R. Sudharsanan, J. W. Eldredge, K. Edmondson, D. E. Joslin *et al.*, Recent developments in high-efficiency $Ga_{0.5}In_{0.5}P/GaAs/Ge$ dual- and triple-junction solar cells: Steps to next-generation PV cells, Sol. Energy Mater. Sol. Cells **66**, 453 (2001).

[5] M. Sytnyk, S. Yakunin, W. Schöfberger, R. T. Lechner, M. Burian, L. Ludescher, N. A. Killilea, A. YousefiAmin, D. Kriegner, J. Stangl *et al.*, Quasi-epitaxial metal-halide perovskite ligand shells on PbS nanocrystals, ACS Nano **11**, 1246 (2017).

[6] C. Cornet, Y. Léger, and C. Robert, *Integrated Lasers on Silicon* (ISTE Press Ltd., London, 2016).

[7] C. Cornet, S. Charbonnier, I. Lucci, L. Chen, A. Létoublon, A. Alvarez, K. Tavernier, T. Rohel, R. Bernard, J.-B. Rodriguez *et al.*, Zinc-blende group III-V/group IV epitaxy: Importance of the miscut, Phys. Rev. Mater. **4**, 053401 (2020).

[8] M. Rio Calvo, J.-B. Rodriguez, C. Cornet, L. Cerutti, M. Ramonda, A. Trampert, G. Patriarche, and É. Tournié, Crystal

phase control during epitaxial hybridization of III-V semiconductors with silicon, Adv. Electron. Mater. **8**, 2100777 (2022).

[9] L. Chen, Y. Léger, G. Loget, M. Piriyev, I. Jadli, S. Tricot, T. Rohel, R. Bernard, A. Beck, J. Le Pouliquen *et al.*, Epitaxial III–V/Si vertical heterostructures with hybrid 2D-semimetal/semiconductor ambipolar and photoactive properties, Adv. Sci. **9**, 2101661 (2022).

[10] P. Kumar and C. H. Patterson, Dielectric Anisotropy of the Gap /Si (001) Interface from First-Principles Theory, Phys. Rev. Lett. **118**, 237403 (2017).

[11] O. Supplie, S. Brückner, O. Romanyuk, H. Döscher, C. Höhn, M. M. May, P. Kleinschmidt, F. Grosse, and T. Hannappel, Atomic scale analysis of the GaP/Si(100) heterointerface by *in situ* reflection anisotropy spectroscopy and *ab initio* density functional theory, Phys. Rev. B **90**, 235301 (2014).

[12] O. Romanyuk, O. Supplie, T. Susi, M. M. May, and T. Hannappel, *Ab initio* density functional theory study on the atomic and electronic structure of GaP/Si(001) heterointerfaces, Phys. Rev. B **94**, 155309 (2016).

[13] A. Beyer, A. Stegmüller, J. O. Oelerich, K. Jandieri, K. Werner, G. Mette, W. Stolz, S. D. Baranovskii, R. Tonner, and K. Volz, Pyramidal structure formation at the interface between III/V semiconductors and silicon, Chem. Mater. **28**, 3265 (2016).

[14] O. Romanyuk, T. Hannappel, and F. Grosse, Atomic and electronic structure of GaP/Si(111), GaP/Si(110), and GaP/Si(113) interfaces and superlattices studied by density functional theory, Phys. Rev. B **88**, 115312 (2013).

[15] M. D. Pashley, Electron counting model and its application to island structures on molecular-beam epitaxy grown GaAs(001) and ZnSe(001), Phys. Rev. B **40**, 10481 (1989).

[16] A. Navarro, E. García-Tabarés, Q. M. Ramasse, P. Caño, I. Rey-Stolle, and B. Galiana, Advanced transmission electron microscopy investigation of defect formation in MOVPE-growth of gap on silicon using arsenic initial coverage, Appl. Surf. Sci. **610**, 155578 (2023).

[17] A. Dupré and P. Dupré, *Théorie Mécanique de la Chaleur* (Gauthier-Villars, Paris, 1869).

[18] See Supplemental Material at http://link.aps.org/supplemental/10.1103/PhysRevB.108.075305 for Bulk crystals and chemical potentials; Stoichiometry; Computational details; H*-passivation methodology; and The phase diagram of GaSiP.

[19] P. Hohenberg and W. Kohn, Inhomogeneous electron gas, Phys. Rev. **136**, B864 (1964).

[20] W. Kohn and L. J. Sham, Self-consistent equations including exchange and correlation effects, Phys. Rev. **140**, A1133 (1965).

[21] J. M. Soler, E. Artacho, J. D. Gale, A. García, J. Junquera, P. Ordejón, and D. Sánchez-Portal, The SIESTA method for *ab initio* order-*N* materials simulation, J. Phys. Condens. Matter **14**, 2745 (2002).

[22] E. Artacho, E. Anglada, O. Diéguez, J. D. Gale, A. García, J. Junquera, R. M. Martin, P. Ordejón, J. M. Pruneda, D. Sánchez-Portal *et al.*, The SIESTA method; developments and applicability, J. Phys. Condens. Matter **20**, 064208 (2008).

[23] J. P. Perdew, K. Burke, and M. Ernzerhof, Generalized Gradient Approximation Made Simple, Phys. Rev. Lett. **77**, 3865 (1996).

[24] N. Troullier and J. L. Martins, Efficient pseudopotentials for plane-wave calculations, Phys. Rev. B **43**, 1993 (1991).

[25] E. Artacho, D. Sanchez-Portal, P. Ordejon, A. Garcia, and J. M. Soler, Linear-scaling *ab-initio* calculations for large and complex systems, Phys. Status Solidi B **215**, 809 (1999).

[26] I. Lucci, S. Charbonnier, M. Vallet, P. Turban, Y. Léger, T. Rohel, N. Bertru, A. Létoublon, J.-B. Rodriguez, L. Cerutti *et al.*, A stress-free and textured GaP template on silicon for solar water splitting, Adv. Funct. Mater. **28**, 1801585 (2018).

[27] N. Moll, A. Kley, E. Pehlke, and M. Scheffler, GaAs equilibrium crystal shape from first principles, Phys. Rev. B **54**, 8844 (1996).

[28] C. Y. Zinchenko, N. L. Shwartz, Z. S. Yanovitskaja, and Y. N. Morokov, *Ab initio* calculations of the Si(001) surface reconstructions using density functional theory, in *International Workshops and Tutorials on Electron Devices and Materials* (IEEE, Piscataway, NJ, 2006), pp. 55–57.

[29] A. Ramstad, G. Brocks, and P. J. Kelly, Theoretical study of the Si(100) surface reconstruction, Phys. Rev. B **51**, 14504 (1995).

[30] V. Kumar and B. S. R. Sastry, Heats of formation of binary semiconductors, Phys. Status Solidi B **242**, 869 (2005).

[31] S. Mirbt, N. Moll, K. Cho, and J. D. Joannopoulos, Cation-rich (100) surface reconstructions of InP and GaP, Phys. Rev. B **60**, 13283 (1999).

[32] K. Luedge, P. Vogt, O. Pulci, N. Esser, F. Bechstedt, and W. Richter, Clarification of the GaP(001)(2 $\times$4) Ga-rich reconstruction by scanning tunneling microscopy and *ab initio* theory, Phys. Rev. B **62**, 11046 (2000).

[33] H. Döscher and T. Hannappel, *In situ* reflection anisotropy spectroscopy analysis of heteroepitaxial GaP films grown on Si(100), J. Appl. Phys. **107**, 123523 (2010).

[34] O. Supplie, M. M. May, H. Stange, C. Höhn, H.-J. Lewerenz, and T. Hannappel, Materials for light-induced water splitting: *In situ* controlled surface preparation of GaPN epilayers grown lattice-matched on Si(100), J. Appl. Phys. **115**, 113509 (2014).

[35] M. M. May, O. Supplie, C. Höhn, R. van de Krol, H.-J. Lewerenz, and T. Hannappel, The Interface of GaP(100) and H_2O studied by photoemission and reflection anisotropy spectroscopy, New J. Phys. **15**, 103003 (2013).

[36] O. Pulci, K. Lüdge, P. Vogt, N. Esser, W. G. Schmidt, W. Richter, and F. Bechstedt, First-principles study of InP and GaP(001) surfaces, Comput. Mater. Sci. **22**, 32 (2001).

[37] K. Jacobi, J. Platen, and C. Setzer, Structure and surface core-level shifts of GaAs surfaces prepared by molecular-beam epitaxy, Phys. Status Solidi B **218**, 329 (2000).

[38] L. Geelhaar, J. Márquez, P. Kratzer, and K. Jacobi, GaAs(2511): A New Stable Surface within the Stereographic Triangle, Phys. Rev. Lett. **86**, 3815 (2001).

[39] Y. Temko, L. Geelhaar, T. Suzuki, and K. Jacobi, Step structure on the GaAs(2511) surface, Surf. Sci. **513**, 328 (2002).

[40] K. Jacobi, L. Geelhaar, and J. Márquez, Structure of high-index GaAs surfaces—The discovery of the stable GaAs (2511) surface, Appl. Phys. A **75**, 113 (2002).

[41] R. Méndez-Camacho, V. H. Méndez-García, M. López-López, and E. Cruz-Hernández, New orientations in the stereographic triangle for self-assembled faceting, AIP Adv. **6**, 065023 (2016).

[42] C. Robert, C. Cornet, P. Turban, T. Nguyen Thanh, M. O. Nestoklon, J. Even, J. M. Jancu, M. Perrin, H. Folliot, T. Rohel *et al.*, Electronic, optical, and structural properties of

(In,Ga)As/GaP quantum dots, Phys. Rev. B **86**, 205316 (2012).
[43] N. Moll, M. Scheffler, and E. Pehlke, Influence of surface stress on the equilibrium shape of strained quantum dots, Phys. Rev. B **58**, 4566 (1998).
[44] W. Ranke and K. Jacobi, Structure and reactivity of GaAs surfaces, Prog. Surf. Sci. **10**, 1 (1981).
[45] C. B. Duke, Semiconductor surface reconstruction: The structural chemistry of two-dimensional surface compounds, Chem. Rev. **96**, 1237 (1996).
[46] I. W. Yeu, G. Han, J. Park, C. S. Hwang, and J.-H. Choi, Equilibrium crystal shape of GaAs and InAs considering surface vibration and new (111)B reconstruction: *Ab-initio* thermodynamics, Sci. Rep. **9**, 1127 (2019).
[47] O. Romanyuk, P. Mutombo, and F. Grosse, *Ab initio* study of atomic disorder on As-Rich GaAs(111)A surface, Surf. Sci. **641**, 330 (2015).
[48] Y. Zhang, J. Zhang, K. Tse, L. Wong, C. Chan, B. Deng, and J. Zhu, Pseudo-hydrogen passivation: A novel way to calculate absolute surface energy of zinc blende (111)/($\overline{1}\overline{1}\overline{1}$) surface, Sci. Rep. **6**, 20055 (2016).
[49] Yu. G. Galitsyn, V. G. Mansurov, I. I. Marahovka, and I. P. Petrenko, Commensurate and incommensurate indium phases on a (111)A InAs surface, Semiconductors **32**, 78 (1998).
[50] J. Yang, C. Nacci, J. Martínez-Blanco, K. Kanisawa, and S. Fölsch, Vertical manipulation of native adatoms on the InAs(111)A surface, J. Phys. Condens. Matter **24**, 354008 (2012).
[51] D. J. Chadi, Vacancy-Induced 2×2 Reconstruction of the Ga(111) Surface of GaAs, Phys. Rev. Lett. **52**, 1911 (1984).
[52] K. W. Haberern and M. D. Pashley, GaAs(111)A-(2 × 2) reconstruction studied by scanning tunneling microscopy, Phys. Rev. B **41**, 3226 (1990).
[53] E. Kaxiras, Y. Bar-Yam, J. D. Joannopoulos, and K. C. Pandey, Variable Stoichiometry Surface Reconstructions: New Models for GaAs($\overline{1}\overline{1}\overline{1}$) (2×2) and ($\sqrt{19}\times\sqrt{19}$), Phys. Rev. Lett. **57**, 106 (1986).
[54] A. Ohtake, J. Nakamura, T. Komura, T. Hanada, T. Yao, H. Kuramochi, and M. Ozeki, Surface structures of GaAs{111}A,B − (2 × 2), Phys. Rev. B **64**, 045318 (2001).
[55] G. Xu, W. Y. Hu, M. W. Puga, S. Y. Tong, J. L. Yeh, S. R. Wang, and B. W. Lee, Atomic geometry of the (2 × 2) GaP(111) surface, Phys. Rev. B **32**, 8473 (1985).
[56] J. H. Poynting and S. J. J. Thomson, *A Text-Book of Physics: Properties of Matter*, 11th ed. (C. Griffin & Company, London, 1913).
[57] K. L. Johnson, K. Kendall, A. D. Roberts, and D. Tabor, Surface energy and the contact of elastic solids, Proc. R. Soc. Lond. A **324**, 301 (1971).
[58] T. Hannappel, O. Supplie, S. Bruckner, M. M. May, P. Kleinschmidt, and O. Romanyuk, Comment on pyramidal structure formation at the interface between III/V semiconductors and silicon, arXiv:1610.01758 (2016).
[59] A. Ponchet, G. Patriarche, J. B. Rodriguez, L. Cerutti, and E. Tournié, Interface energy analysis of III–V islands on Si(001) in the Volmer-Weber growth mode, Appl. Phys. Lett. **113**, 191601 (2018).
[60] R. Hull and A. Fischer-Colbrie, Nucleation of GaAs on Si: Experimental evidence for a three-dimensional critical transition, Appl. Phys. Lett. **50**, 851 (1987).
[61] F. Ernst and P. Pirouz, Formation of planar defects in the epitaxial growth of GaP on Si substrate by metal organic chemical-vapor deposition, J. Appl. Phys. **64**, 4526 (1988).
[62] P. Müller and R. Kern, Equilibrium shape of epitaxially strained crystals (Volmer-Weber case), J. Cryst. Growth **193**, 257 (1998).